Applied Physics Reviews ARTICLE scitation.org/journal/are

Performance boosting strategy for perovskite light-emitting diodes

Cite as: Appl. Phys. Rev. 6, 031402 (2019); doi: 10.1063/1.5098871
Submitted: 4 April 2019 · Accepted: 21 June 2019 ·
Published Online: 30 July 2019

Kihyung Sim,[1] Taehwan Jun,[1] Joonho Bang,[1] Hayato Kamioka,[2] Junghwan Kim,[1,a)] Hidenori Hiramatsu,[1,3] and Hideo Hosono[1,3,a)]

AFFILIATIONS

[1]Materials Research Center for Element Strategy, Tokyo Institute of Technology, Mailbox SE-1, 4259 Nagatsuta, Midori-ku, Yokohama 226-8503, Japan
[2]Department of Physics, College of Humanities and Sciences, Nihon University, 3-25-40 Sakurajyousui, Setagaya-ku, Tokyo 156-8550, Japan
[3]Laboratory for Materials and Structures, Institute of Innovative Research, Tokyo Institute of Technology, 4259 Nagatsuta, Midori-ku, Yokohama 226-8503, Japan

[a)]Authors to whom correspondence should be addressed: JH.KIM@mces.titech.ac.jp and hosono@msl.titech.ac.jp

ABSTRACT

Low-dimensional (low-D) luminescent materials have attracted significant attention due to the high photoluminescent quantum yields. However, it is unclear whether low-D materials are superior to 3D materials for electroluminescent (EL) devices given that low-D materials have poor charge transport nature due to their highly localized electronic structures. We noticed a significant phenomenon that EL performances for 3D materials, such as $CsPbX_3$, are governed by adjacent charge transport layers, which is possibly due to nonradiative recombination resulting from the small exciton binding energy. This finding encouraged us to develop new electron transport layers (ETLs) that satisfy not only the energy alignment to confine excitons but also an efficient electron injection into 3D $CsPbX_3$ layers. This strategy enables one to exploit the good charge transport nature of 3D $CsPbX_3$. The proposed amorphous Zn-Si-O ETL has sufficiently shallow electron affinity (~3.2 eV) to confine excitons and sufficiently high electron mobility (~0.8 $cm^2/V\,s$) to transport electrons. Furthermore, the controllable conductivity and electron affinity of amorphous Zn-Si-O enable fine-tuning of charge balance. Consequently, the very low operating voltage of 2.9 V at 10 000 cd/m^2 and high power efficiency of 33 lm/W were achieved for a green perovskite ($CsPbBr_3$) EL (PeLED). The obtained ultrahigh brightness of ~500 000 cd/m^2 demonstrates the effectiveness of the proposed strategy. We also extend this strategy into 3D $CsPbBrI_2$ (red) and 3D $CsPbBrCl_2$ (blue) PeLEDs, and demonstrate a record high brightness of 20 000 cd/m^2 for the red PeLED. We believe this study provides new insight into the realization of practical PeLEDs.

I. INTRODUCTION

To date, a variety of luminescent materials with high photoluminescence quantum yield (PLQY) have been reported for optoelectronic applications.[1–4] Organic phosphorescent materials for organic light emitting diodes (OLEDs) have achieved internal quantum efficiency of ~100%.[3,4] While the high PLQY is certainly a factor, this does not always guarantee highly efficient electroluminescent (EL) devices. In 1987, Tang *et al.*[5] demonstrated the first OLED employing Alq3 as an emission layer (EML), which had a power efficiency of 1.5 lm/W. Recent OLEDs with Alq3 exhibit much higher power efficiency, i.e., ~4.5 lm/W. In other words, based on the same EML, power efficiency has improved by a factor of 3 over the past three decades. Such improvement has been realized with a variety of functional materials, such as charge injection/transport layers, and has contributed to the comprehensive understanding of EL devices. On the other hand, metal halide perovskites, such as $CsPbX_3$ (X: I, Br, and Cl), have emerged recently as promising candidates for EMLs due to their promising optical properties,[6–8] i.e., very narrow full width at half maximum (FWHM), solution processability, and low-cost fabrication processes. However, the performance of $CsPbX_3$-based ELs (PeLEDs) remains insufficient compared to conventional OLEDs. To improve the EL performance, many studies have proposed the use of low-dimensional

(low-D) perovskites or quantum dots (QDs). In fact, the very high PLQYs exhibited are attributable to the quantum confinement effect (QCE) (e.g., exciton binding energy of ~35 meV for $CsPbBr_3$[9] and ~350 meV for 0D Cs_4PbBr_6[10]). Although the exciton binding energy of GaN is only ~20 meV, the GaN-based LEDs exhibit very high efficiency (>160 lm/W).[11] Thus, it remains uncertain whether low-D materials with high QCEs are essential to realize efficient EL devices. There are several criteria to satisfy for an efficient EL: (i) a high PLQY emission layer, (ii) efficient electron and hole injection and transport layers, (iii) high light outcoupling efficiency, etc. Generally, low-D or QD materials are unfavorable for exhibiting good charge transport properties due to their strongly localized electronic structure (i.e., the large effective mass of the electron/hole). Figure 1 schematically describes the different natures of 3D (e.g., $CsPbBr_3$) and low-D materials with respect to exciton binding energy and charge transport properties. Note that there is a trade-off between exciton binding energy and charge transport. Generally, 3D materials have superior carrier transport ability; however, non-radiative recombination tends to readily occur due to their small exciton binding energy. In contrast, low-D materials demonstrate high PLQYs but poor charge transport characteristics. Therefore, a strategy to overcome this trade-off relationship is in high demand.

EL devices, such as OLEDs, comprise several functional layers [e.g., the electron transport layer (ETL), the EML, and the hole transport layer (HTL)], which is a two-dimensional architecture where an ETL and HTL confine the EML. Thus, the whole device structure can be regarded as a scaled-up low-D material if the ETL and HTL have the energy levels to sufficiently confine electrons and holes, as shown in Fig. 1(d). In other words, the conduction band minimum level (E_{CBM}) and valence band maximum level (E_{VBM}) of the ETL/HTL should be shallower and deeper than those of the EML, respectively. However, it is rather difficult to obtain ETL/HTL materials that satisfy

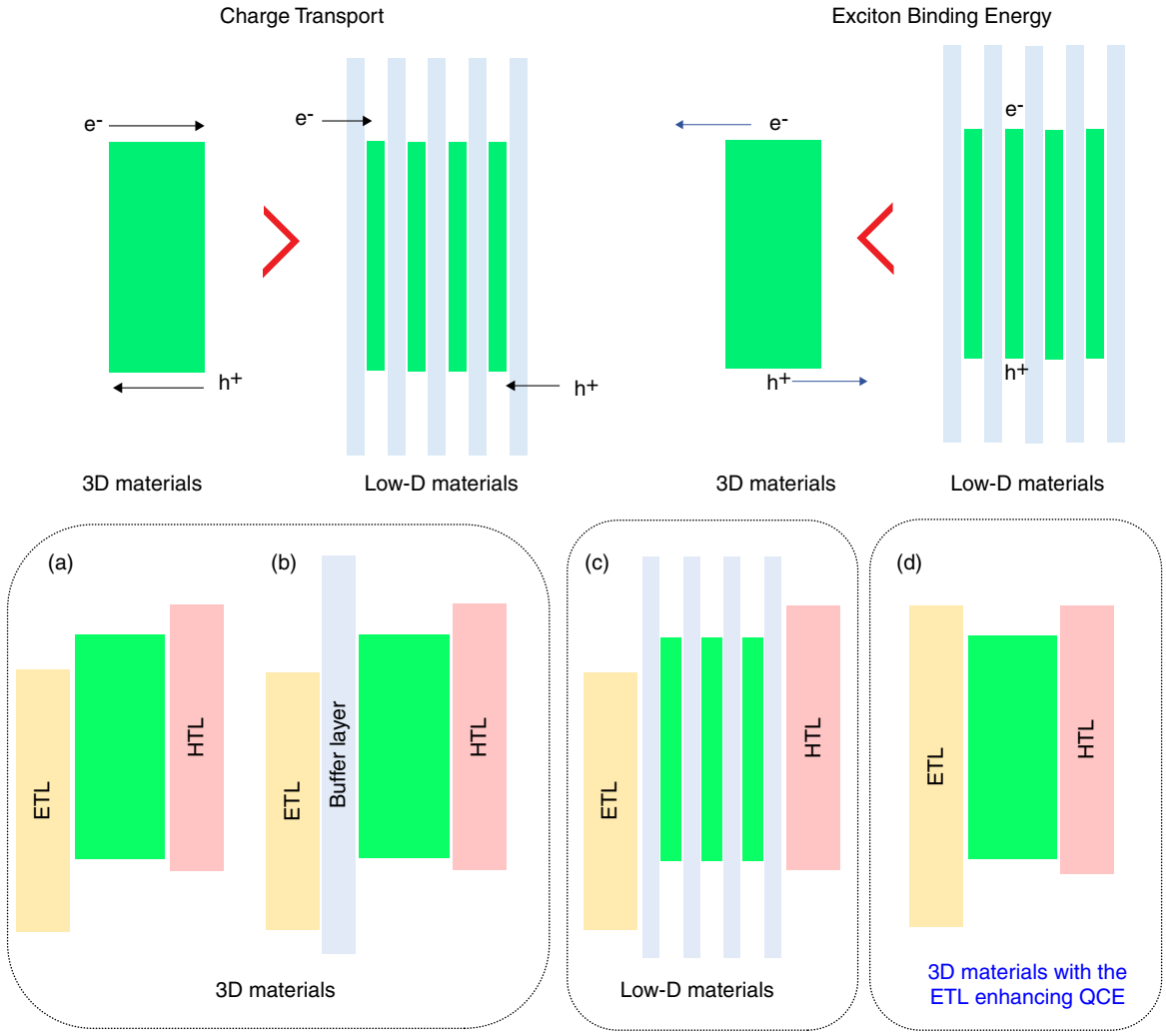

FIG. 1. Charge transport properties and exciton binding energy of 3D materials and low-D materials. Comparison of conventional device structures for 3D [(a) and (b)] and low-D (c). (d) Proposed energy alignment of 3D materials with ETL or HTL.

both energy alignment and charge transportability. Consequently, either Fig. 1(a) or 1(c) becomes the most common structure, which leads to low-D ELs that are superior to 3D ELs.

Recently, Zhang *et al.* compared PeLEDs relative to the device structures shown in Figs. 1(a) and 1(b).[12] The maximum luminance (L_{max}) and current efficiency were improved by inserting a polyvinyl pyrrolidine buffer layer between ZnO ETL and $CsPbBr_3$ EML. L_{max} increased from 350 to 11 600 cd/m^2 while current efficiency improved from 0.26 to 7.19 cd/A. They suggested two possible reasons for this result, i.e., (i) suppression of the pinhole and (ii) improved charge balance. However, these reasons are insufficient to explain another experimental result, i.e., deterioration in photoluminescent (PL) lifetime for ZnO/$CsPbBr_3$, because both the pinhole and charge balance should only primarily affect the EL performance, not PL lifetime. Here, we focus on the possibility of nonradiative recombination (exciton quenching) resulting from energy-level alignments between $CsPbBr_3$ and neighboring layers and propose a strategy to realize highly efficient PeLEDs.

II. SIGNIFICANCE OF ENERGY-LEVEL ALIGNMENT IN 3D PeLEDS

A. Discovered exciton quenching phenomenon owing to adjacent layers

Amorphous oxide semiconductors (AOS) have a variety of advantageous properties for electronic devices, such as low-temperature processability, good uniformity, high transparency, and high mobility.[13] Wide tunability in chemical composition enables continuous modification of their electronic structures and electrical properties.[14] Generally, post-transition metal oxide semiconductors have a deep E_{VBM} of ~7 eV; thus, it is expected that such oxide materials sufficiently block the holes from $CsPbBr_3$ (I.P. of $CsPbBr_3$ is ~5.6 eV). The E_{CBM} of $CsPbBr_3$ is rather shallower than those of oxide semiconductors (3.3 eV for $CsPbBr_3$ and 4.5 eV for ZnO). Therefore, electron-hole pairs can readily dissociate at the interface between oxide semiconductor and $CsPbBr_3$. Note that such electron-hole dissociation is strongly related to the exciton binding energy, as described in Fig. 1, and this phenomenon is similar to the correlation between exciton binding energy and electron-hole diffusion length or short-circuit current for photovoltaic materials.[15]

To confirm how the energy alignment of $CsPbBr_3$ with neighboring layers affects PL or EL devices, we prepared several AOSs with different E_{CBM} values. Here, ZnO was chosen and modified to an amorphous Zn-Si-O (a-ZSO) system.[16] a-ZSO thin films (120-nm thick) of different Zn/(Zn + Si) ratio (90%, 85%, 80%, and 75%) were deposited on glass substrates using RF magnetron sputtering at room temperature. Figure 2 summarizes their optical bandgap, electrical conductivities, and energy levels. For AOSs, the vacant s orbitals of metal cations primarily control the CBM. The optical bandgap of a-ZSO increases with increasing the Si content, while electrical conductivity decreases and E_{CBM} (electron affinity) becomes shallow. The CBM of a-ZSO is mainly formed by 4s orbitals of Zn^{2+} ions. Therefore, conduction band dispersion is suppressed when Si content increases, resulting in the shallow E_{CBM} and a wider optical bandgap. Note that the E_{CBM} of a-ZSO becomes close to that of $CsPbBr_3$ when Si content is ~15% [Fig. 2(c)].

$CsPbBr_3$ thin films were spin-coated on glass substrates onto which ITO and a-ZSO were deposited. The energy levels of the relevant materials are summarized in Fig. 3(a). Time-resolved PL spectra were measured (see Fig. S1 in the supplementary material), and PL lifetimes were determined from the obtained PL decay curves. As shown in Fig. 3(b), a noticeable correlation can be observed between the energy alignments and PL lifetime. The $CsPbBr_3$ on ITO exhibited the shortest PL lifetime, which agrees well with the photograph. Here, very weak emission was observed under UV light excitation for the sample on the ITO. On the other hand, the PL lifetime increased and saturated at ~17 ns with increasing Si content of a-ZSO. Nearly the same value (~17 ns) was confirmed for the sample deposited on bare glass substrate, which implies that the a-ZSO (Si ≥ 20%) possesses an adequate energy level to confine excitons in $CsPbBr_3$, and corresponds well to the energy-level alignments shown in Figs. 2(c) and 3(a). To investigate the PL dependence of low-D materials on the energy-level alignment with neighboring layers, we employed a $Cs_3Cu_2I_5$ with a zero-dimensional (0D) photoactive site and very large exciton binding energy of ~490 meV.[1] As shown in Fig. 3(c), all $Cs_3Cu_2I_5$ thin films exhibited bright emission regardless of the neighboring layer. These results clarify that the luminescent material with larger exciton binding energy is less sensitive to its neighboring layers.

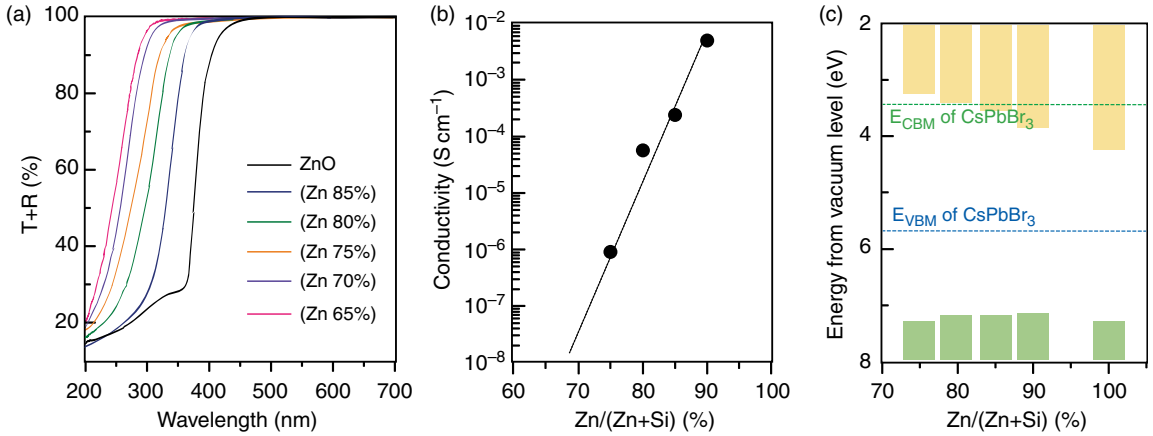

FIG. 2. (a) Optical properties, (b) electrical conductivities at RT, and (c) energy levels are compared for a-ZSO thin films as a function of Zn/(Zn + Si) ratio.

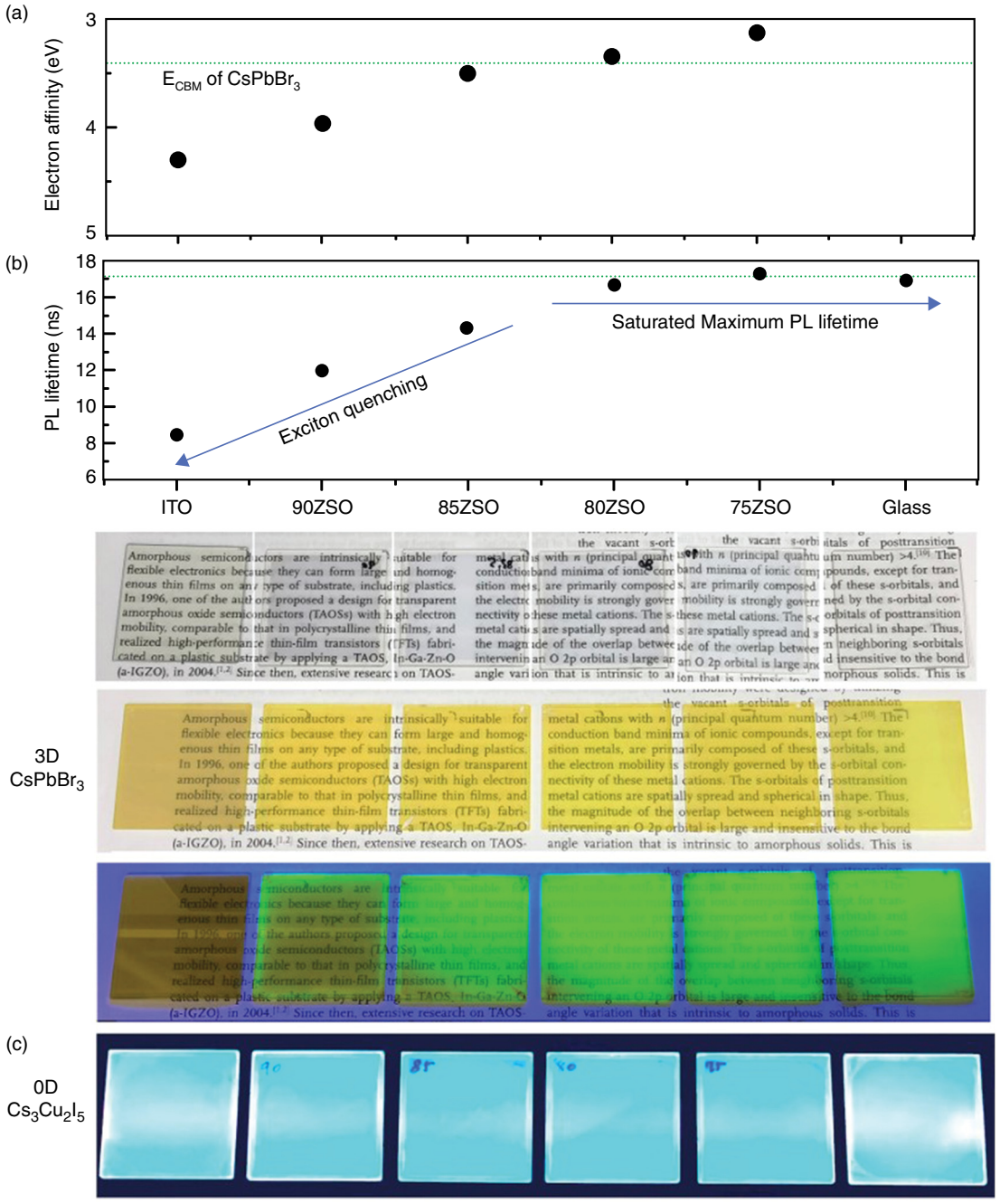

FIG. 3. (a) Electron affinity values of ITO, 90ZSO, 85ZSO, 80ZSO, and 75ZSO. (b) PL lifetimes and photo of PL from $CsPbBr_3$ thin films fabricated on ITO, 90ZSO, 85ZSO, 80ZSO, 75ZSO, and bare glass substrates. (c) Photograph of $Cs_3Cu_2I_5$ thin films on each substrate under UV light excitation.

B. Enhanced exciton confinement effect utilizing charge transport layers

As discussed previously, a-ZSO exhibits good energy alignment with $CsPbBr_3$ and good electrical properties. Hall measurement results demonstrated that the electron mobility and carrier density of a-ZSO with Zn/(Zn + Si):80% (80ZSO) were 0.8 cm^2/V s and 4×10^{13} cm^{-3}, respectively. Furthermore, a-ZSO exhibits strong chemical stability against solvents. As shown in Fig. 4, the electrical conductivities of the 80ZSO thin film before and after spin-coating were similar, which indicates the wide applicability of a-ZSO to various solution-processable optoelectronic devices. To confirm the ability of a-ZSO as

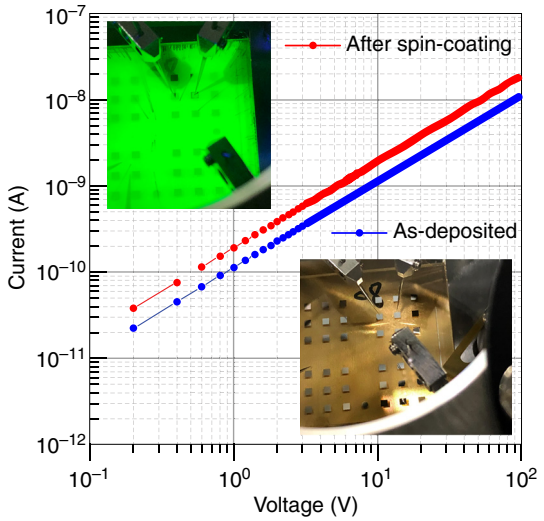

FIG. 4. Stability of current–voltage (I–V) characteristics of 120-nm thick 80ZSO against $CsPbBr_3$ precursor solvent. Photo at bottom-right shows the stability of a-ZSO after the spin-coated $CsPbBr_3$ layer was removed by washing with pure water.

an ETL, we fabricated PeLEDs of 1 mm × 1 mm with the inverted structure shown in Fig. 5(a) [ITO (150 nm)/80ZSO (120 nm)/$CsPbBr_3$ (60 nm)/NPD (40 nm)/MoO_x (5 nm)/Ag (100 nm)]. The $CsPbBr_3$ thin film was spin-coated on the 120-nm thick 80ZSO ETL [Fig. 5(b)] in a globe box filled with Ar gas. As shown in Fig. 5(c), the fabricated $CsPbBr_3$ thin films are very uniform in the whole area of 3 cm × 3 cm. NPD and MoO_x were thermally evaporated as an HTL and hole injection layer (HIL), respectively. The PeLED with the 80ZSO ETL shows an EL peak at ∼523 nm with a full width at half maximum (FWHM) of 16 nm [Fig. 5(d)], which is nearly the same as the PL spectrum. On the other hand, the high luminous intensity was confirmed at a rather low operating voltage, i.e., 10 000 cd/m^2 at 2.9 V and 120 000 cd/m^2 at 4 V [Fig. 5(e)]. Due to the low operating voltage, a high power efficiency of ∼25 lm/W was achieved [Fig. 5(f)], while significantly high brightness (180 000 cd/m^2) was confirmed at 5 V, as shown in Fig. 5(e). The L_{max} further increased to 500 000 cd/m^2 using a bilayered HTL of CBP 20 nm/NPD 20 nm (see Fig. S2 in the supplementary material), while current efficiency and power efficiency increased to 37 cd/A and 33 lm/W, respectively. This high brightness substantiates efficient charge injection into $CsPbBr_3$ and good charge balance, which can also be concluded from the obtained external quantum efficiency (EQE) of ∼10% which is a high value among the recently reported green PeLEDs based on the same $CsPbBr_3$ (Table I). On the other hand, recent works show that organometal halide perovskites exhibit much higher EQEs than inorganic $CsPbBr_3$; a quite high EQE of ∼20% was achieved using $MA_xCs_{1-x}PbBr_3$.[26] It is inferred that EQE is

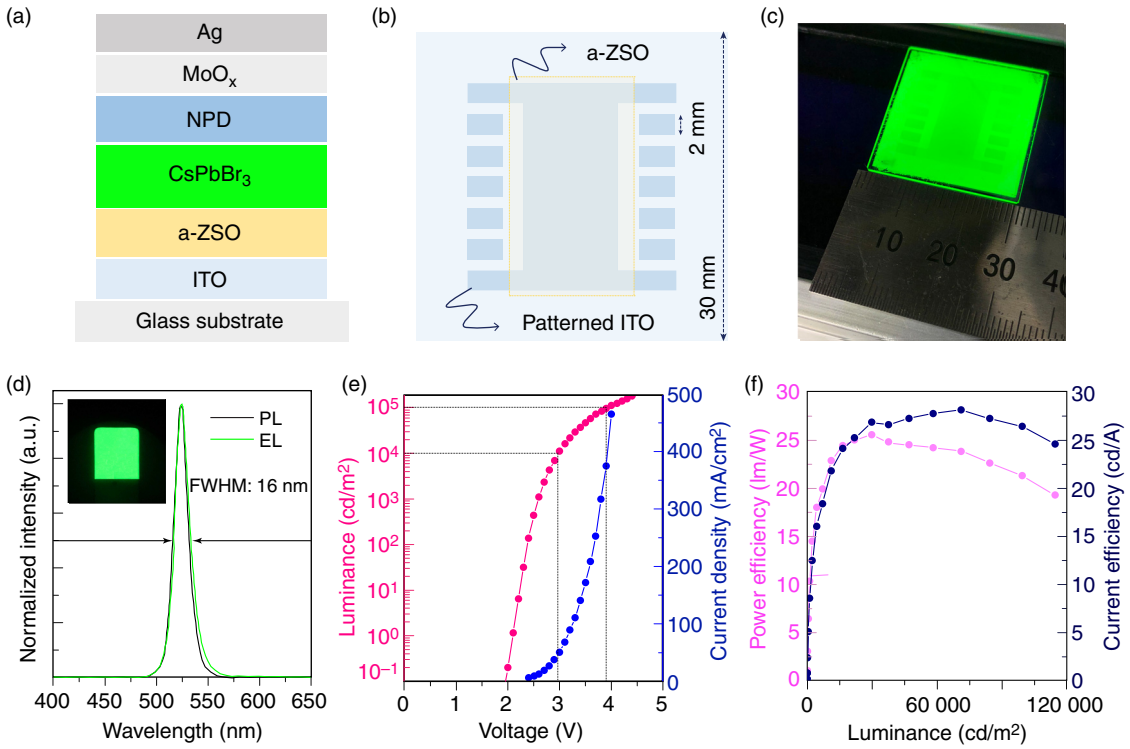

FIG. 5. (a) Device structure of PeLED and (b) ITO-patterned glass substrate onto which 80ZSO thin film was deposited as ETL. (c) Photograph of spin-coated $CsPbBr_3$ thin film on 80ZSO ETL (UV excitation: 365 nm). (d) Comparison of photoluminescence and electroluminescence spectra. (e) Luminance–current density–voltage characteristic. (f) Power efficiency (lm/W) and current efficiency (cd/A) of the PeLED with 80ZSO ETL.

TABLE I. EL performance of recent green PeLEDs [operating voltage, maximum luminance (L_{max}), maximum current efficiency ($C.E._{max}$), maximum power efficiency (P.E.), and maximum external quantum efficiency (EQE_{max})].

EML materials	Voltage (V) at 10^3, 10^4 cd/m^2	L_{max} (cd/m$^{2)}$	$C.E._{max}$ (cd/A)	P.E. (lm/W)	EQE_{max} (%)	References
$CsPbBr_3$	2.5, 2.9	496 320	37	33	9.3	This work
$CsPbBr_3$	4.2, 5.2	51 890	21.4	14.9	4.76	17
$CsPbBr_3$	3.75, 5	23 828	9.5	5.4	2.94	18
$CsPbBr_3$	3.1, 4.1	53 525	15.7	12.3[a]	4.26	19
$FA_xCs_{1-x}PbBr_3$	9.3, 17.6	9 834	14.5	3.4[a]	3.1	20
$MAPbBr_3$	4.6, 5.75	…	18	8.7[a]	3.8	21
$MAPbBr_3$	5.55, 8.35	20 000	42.9	15[a]	8.53	22
$MA_xCs_{1-x}PbBr_3$	3.2, 4.3	14 000	80	69	20	26
$MA_xCs_{1-x}PbBr_3$	4.8, 6.3	91 000	33.9	17.8[a]	10.4	12
2D BABr-$CsPbBr_3$	3.85, 4.8	33 532	25.1	18.3[a]	8.42	23
$CsPbBr_3$ QDs	4.1, …	1660	26.2	31.7	8.73	24
$CsPbBr_3$ QDs	6.2, 10.5	10 206	8.73	2.5[a]	4.63	25

[a]Estimated by the authors from L–J–V and C.E. data in the relevant references.

governed primarily by EML materials. Herein, it should be noted that EQE is a factor to evaluate the EML rather than the EL performance. For EL devices, power efficiency should be considered because it reflects both EQE and operating voltage. The significance of the operating voltage is suggested from the fact that the organometal halide-based PeLEDs[12,22,23] with similar EQEs of ∼10% exhibit much lower power efficiencies than our 33 lm/W due to its high operating voltage (Table I). This result demonstrates the critical importance of maintaining a balance between the luminescent and electronic transport properties to achieve high EL performance.

Next, we also confirmed the stability of the green PeLED with the a-ZSO ETL. Figure 6(a) shows a stable EL performance against repeated measurements in the high luminance region; L–V characteristic remained unchanged up to ∼40 000 cd/m^2. Operational lifetime was also measured as shown in Figs. 6(b)–6(d). Even under high-brightness operation, relatively long half-lifetimes (T_{50}) were confirmed (Table SII in the supplementary material).

Generally, an electron injection barrier arises between the cathode electrode and ETL, as shown in Fig. S3(a) in the supplementary material. Note that electron injection layers (EILs) have been widely used to reduce the height of the electron injection barrier [Fig. S3(b) in the supplementary material]. In contrast, a-ZSO can make a quasi-Ohmic contact with cathode materials, such as Al and ITO, regardless of its shallow E_{CBM}, which enables the transport of electrons from the cathode to the EML with no injection barrier height [Fig. S3(c) in the supplementary material].[16] This unique property of a-ZSO plays an important role in realizing low operating voltage and the simplification of the fabrication process by omitting EILs.

III. SIGNIFICANCE OF CHARGE BALANCE IN 3D PeLEDS

Next, we investigated how the charge balance affects the performance of the PeLEDs. As shown in Fig. 2(b), the electrical property of a-ZSO varies according to the Zn/(Zn + Si) ratio. Figures 7(a) and 7(b) compare the luminance–current density–voltage (L–J–V) characteristics of the PeLEDs with 85ZSO, 80ZSO, 75ZSO, and 70ZSO ETLs. The PeLEDs using 85ZSO and 80ZSO ETLs exhibit similar L–V characteristics; however, the PeLED with the 85ZSO ETL shows much higher current density than that with 80ZSO. As a result, the PeLED with 85ZSO shows

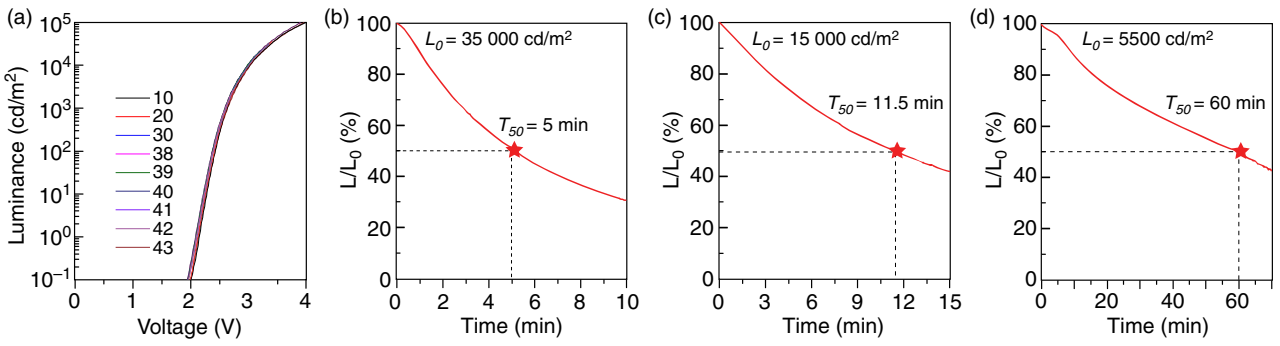

FIG. 6. (a) Luminance–voltage characteristics of green PeLED with the 80ZSO ETL as a function of the number of measurements. Operational stability at different L_0 (initial luminance): (b) 35 000 cd/m^2, (c) 15 000 cd/m^2, (d) 5500 cd/m^2. The half-lifetime (T_{50}) was defined as the time taken for L_0 decreasing to 50%.

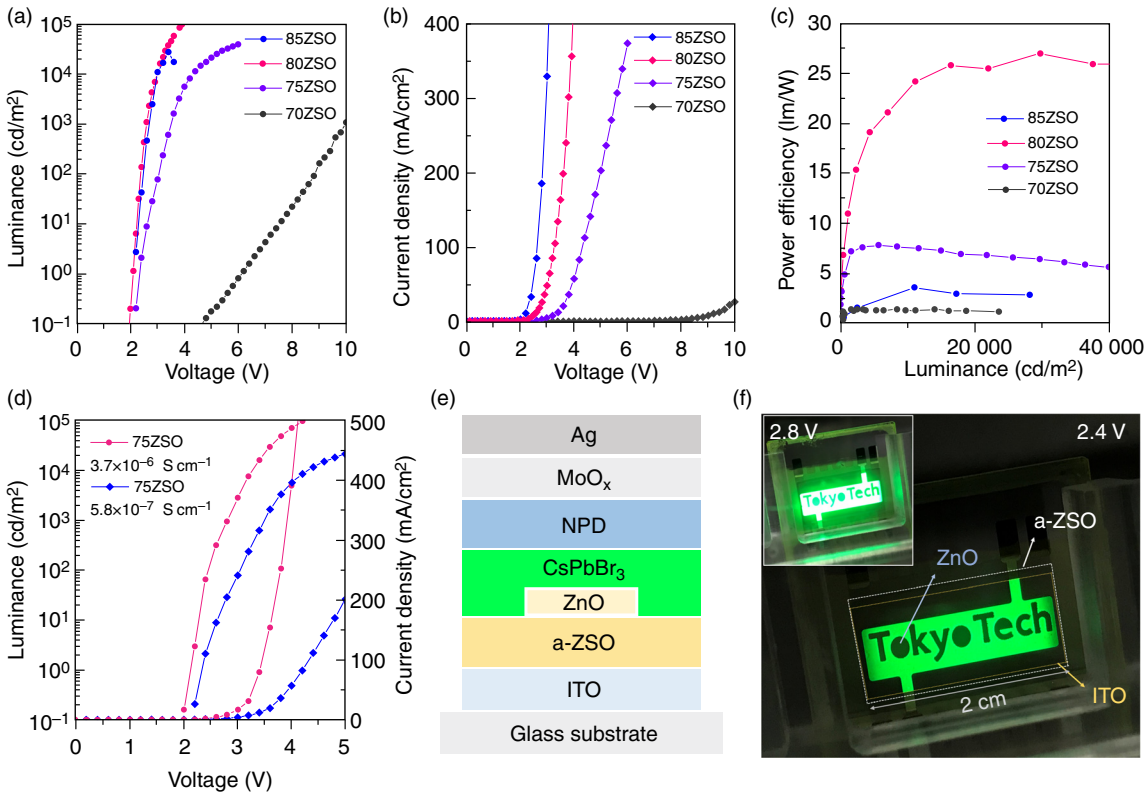

FIG. 7. EL performance of PeLEDs with a-ZSO of different Zn content (85ZSO, 80ZSO, 75ZSO, and 70ZSO). Comparison of (a) luminance–voltage, (b) current density–voltage characteristics, and (c) power efficiency. (d) EL performance of PeLEDs using 75ZSO ETLs with different conductivities. (e) Device structure of large PeLED (20 mm × 5 mm) with Tokyo Tech patterning, where a 20-nm thick ZnO layer was deposited on the a-ZSO ETL. (f) Photograph of large PeLED at 2.4 and 2.8 V.

very low efficiency and broke down at the low voltage region of ~3 V, which corresponds to that discussed previously relative to the correlation between charge balance and L_{max}. The effect of the electrical properties of the ETLs was observed more clearly from a comparison on PeLEDs with 75ZSO and 70ZSO. The 75ZSO showed conductivity of 5.8×10^{-7} S cm^{-1}, while we could not evaluate the conductivity of the 70ZSO due to its rather high resistivity. Corresponding to their electrical conductivities, the operating voltage increased and power efficiency decreased. These results appear reasonable in terms of charge balance and/or series resistance.

To demonstrate the advantage of using the a-ZSO ETL, we also performed conductivity fine-tuning for the 75ZSO ETL, where the conductivity of AOSs can be readily controlled by sputtering parameters, such as partial oxygen pressure and RF power. As shown in Fig. 7(d), the operating voltage decreased and current density increased by increasing the conductivity of 75ZSO from 5.8×10^{-7} to 3.7×10^{-6} S cm^{-1}, and the power efficiency increased from 7.5 to 22 lm/W. This result demonstrates that usage of a transparent amorphous oxide semiconductor ETL, such as a-ZSO, will be advantageous relative to optimizing the charge balance due to their widely tunable electrical properties. For organic ETL materials, thickness control is the primary method to tune charge balance; however, it is difficult to vary conductivities in a wide range with this method.

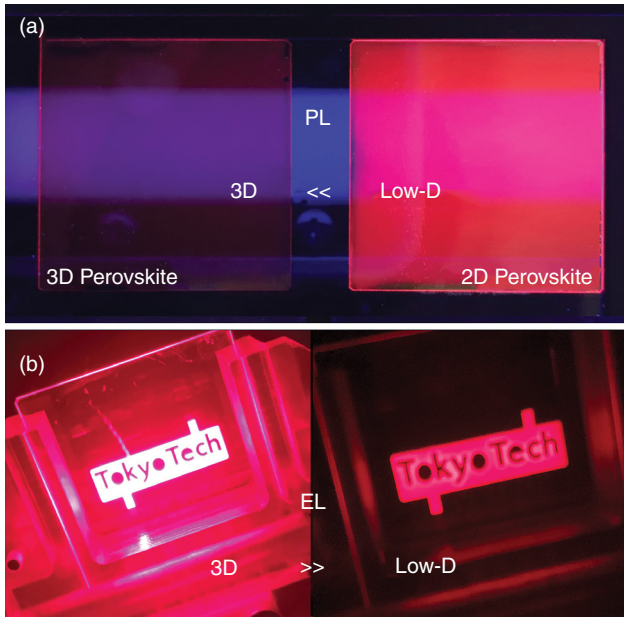

FIG. 8. Photographs of (a) PL and (b) EL for 3D $CsPbBrI_2$ and 2D BAI-$CsPbI_3$, respectively.

A PeLED of 20 mm × 5 mm was fabricated to visualize the significance of this work. The 20-nm thick ZnO thin film was partially deposited on the 80ZSO ETL [Fig. 7(e)]. Here, the series resistance of ZnO was negligible due to its 10 times higher conductivity ($\sim 10^{-4}$ S cm^{-1}) than 80ZSO (10^{-5} S cm^{-1}; carrier density of $\sim 10^{14}$ cm^{-3}). Exciton quenching by free carriers (Auger recombination) was also negligible for ZnO due to the low carrier density of $\sim 10^{15}$ cm^{-3}. As shown in Fig. 7(f), only the area where the 80ZSO ETL was directly adjacent to the $CsPbBr_3$ emits bright green light. In contrast, very weak emission was observed from the area of 20-nm thick ZnO, corresponding to the "Tokyo Tech" region. This result clearly demonstrates the critical role of energy-level alignment.[8]

IV. ULTRAWIDE COLOR GAMUT USING RED, GREEN AND BLUE 3D PeLEDS WITH a-ZSO ETLS

To demonstrate the validity of our strategy, we also fabricated red and blue PeLEDs with the same structure in Fig. 5(a). Here, we chose 3D $CsPbBrI_2$ and 3D $CsPbBrCl_2$ as a red and a blue emitting layer, respectively. The $CsPbBrI_2$ has been extensively studied for perovskite solar cells;[27] a high power conversion efficiency of ~10% was already achieved, which implies that excitons readily dissociate into electrons and holes, and they rapidly transport to cathode and anode. In contrast, these properties will result in poor EL performance without any QCE as illustrated in Fig. 1. Thus, our strategy should be more convincing if a high EL performance is achieved using $CsPbBrI_2$. For comparison, a red PeLED was also fabricated using 2D BAI-$CsPbI_3$.[31] The XRD patterns (Fig. S4 in the supplementary material), EPMA results (Table SIII in the supplementary material), and PL spectrum (Fig. S5 in the supplementary material) show that 3D $CsPbBrI_2$ and 2D BAI-$CsPbI_3$ thin films were successfully fabricated. As seen in Fig. 8(a), it was clearly observed that 2D BAI-$CsPbI_3$ emits much brighter red light than 3D $CsPbBrI_2$ under UV-light excitation. This result agrees well with Ref. 31 and shows that lowering the dimensionality definitely enhances QCE. Then, what about EL performance? As shown in Figs. 8(b) and 9(a), much better EL performance was obtained from the $CsPbBrI_2$ PeLED than the 2D red PeLED. Very low operating voltage and high brightness were confirmed: 2.8 V for 100 cd/m^2, 3.4 V for 1000 cd/m^2 and 4.5 V for 10 000 cd/m^2. The EL peak was at ~650 nm with a FWHM of 40 nm [Fig. 9(b)]. To the best of our knowledge, the obtained L_{max} of 20 000 cd/m^2 is a record high among the red PeLEDs reported to date. It is noticeable that the L_{max} values of most red PeLEDs are lower than 1 000 cd/m^2; the brightness of 1 000 cd/m^2 is still insufficient for practical use (Table SI[28–30,32–42] in the supplementary material).

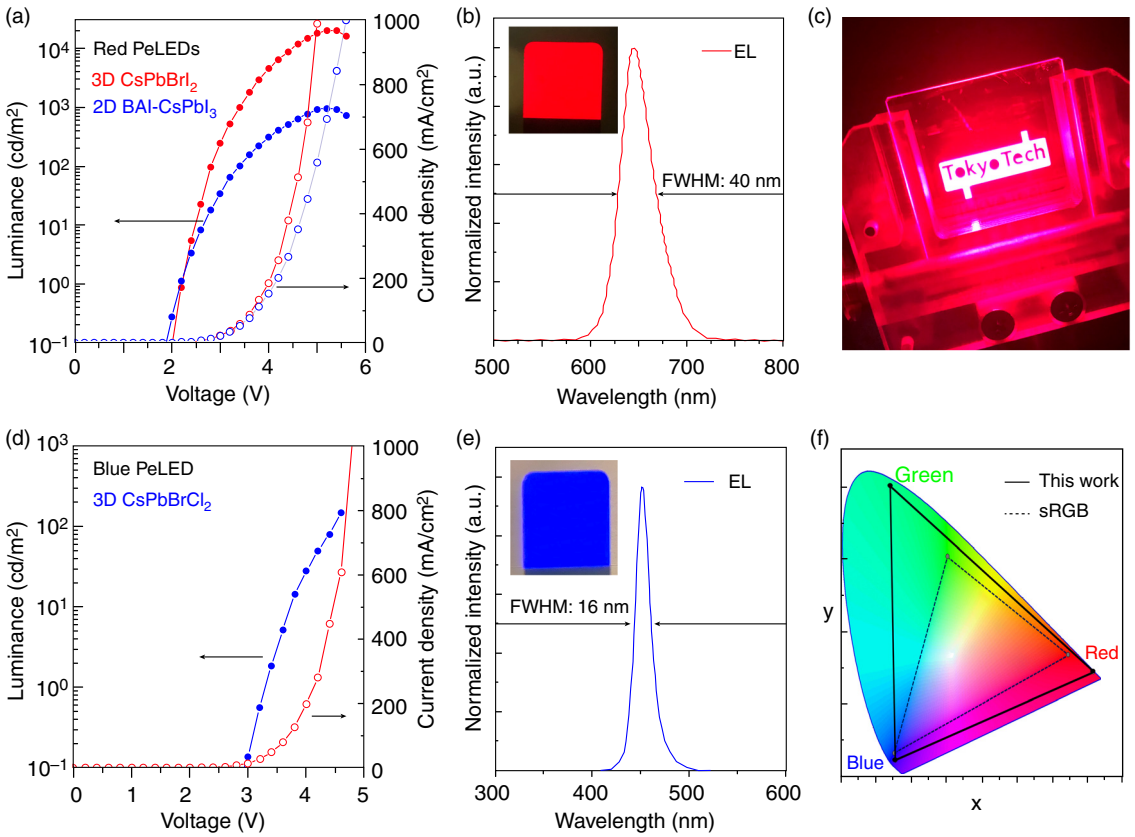

FIG. 9. (a) Luminance–current density–voltage (L–J–V) characteristics of the $CsPbBrI_2$ PeLED and the 2D BAI-$CsPbI_3$ PeLED. (b) EL spectrum and photograph (inset) of $CsPbBrI_2$ PeLED. (c) Large-size PeLED (20 mm × 5 mm) with Tokyo Tech patterning. (d) L–J–V characteristic and (e) EL spectrum and photograph (inset) of the $CsPbBrCl_2$ PeLED. (f) CIE coordination from the obtained EL spectra for red, green, and blue PeLEDs.

A significant improvement in EL performance was also confirmed for the blue PeLED using $CsPbBrCl_2$ [Fig. 9(d)]. The EL peak was at ~452 nm with a FWHM of 16 nm [Fig. 9(e)]. Similar to the red PeLEDs, the EL performance of our blue PeLED using 3D $CsPbBrCl_2$ is better than low-D blue PeLEDs (Table SI in the supplementary material). However, the EL performance of blue PeLEDs is unsatisfactory compared to green and red PeLEDs; the difficulty in hole injection owing to the deep ionization potential of $CsPbBrCl_2$ may be responsible for the poor EL performance.

V. CONCLUSION

In conclusion, we confirmed the significance of obtaining both good charge transportability and quantum confinement effects for boosting the performance of PeLEDs. It was revealed that EL performances for 3D materials, such as $CsPbX_3$, are governed by adjacent charge transport layers, which is possibly due to nonradiative recombination resulting from the small exciton binding energy. The newly developed a-ZSO ETLs enabled us to enhance the exciton confinement effect utilizing the good charge transport nature of 3D $CsPbX_3$. Consequently, significantly high brightness with low operating voltages was realized for green and red PeLEDs. We believe this study provides new insight into the realization of practical PeLEDs.

SUPPLEMENTARY MATERIAL

See the supplementary material for details on device fabrication and measurement, and additional data on chemical composition, PL, EL performance, and so on.

ACKNOWLEDGMENTS

This work was supported by the Ministry of Education, Culture, Sports, Science, and Technology (MEXT) through the Element Strategy Initiative to Form Core Research Center. J.K. was also supported by the Japan Society for the Promotion of Science (JSPS) through a Grant-in-Aid for Young Scientists (Grant No. 19K15655). H. Hi. was also supported by the JSPS through Grants-in-Aid for Scientific Research (A) and (B) (Grant Nos. 17H01318 and 18H01700), and Support for Tokyo Tech Advanced Research (STAR).

APPENDIX: EXPERIMENTAL

1. Fabrication of a-ZSO ETL and characterization

Amorphous Zn–Si–O (a-ZSO) thin films were deposited at room temperature via RF magnetron sputtering using ($ZnO–SiO_2$) 3-in. ceramic targets (Zn:Si = 70:30, 75:25, 80:20, 85:15, and 90:10 at. %). The following sputtering parameters were used: RF power, 80 W; target–substrate distance, 80 mm; total pressure, 0.4 Pa; partial oxygen pressure, 0.25%. The electrical properties of a-ZSO were investigated by AC Field Hall effect measurement (ResiTest8400, Toyo Corp.) under the van der Pauw configuration. The film thickness was determined using grazing-incidence x-ray reflectivity spectroscopy, and the optical bandgap of a-ZSO was estimated from the optical absorption spectra obtained using a UV-Vis spectrometer (UH4150, Hitachi).

2. Synthesis of $CsPbBr_3$, $CsPbBrI_2$, and $CsPbBrCl_2$ thin films and characterization

CsBr (99.999%), $PbBr_2$ (99.999%), PbI_2 (99.99%), and $PbCl_2$ (99.999%) powders were purchased from Sigma-Aldrich. The precursor solutions were prepared by dissolving CsBr and ($PbBr_2$ or PbI_2 or $PbCl_2$) in DMSO for $CsPbBr_3$ (CsBr: $PbBr_2$, molar ratio of 1.05:1), $CsPbBrI_2$ (CsBr: PbI_2, molar ratio of 1.05:1), and $CsPbBrCl_2$ (CsBr: $PbCl_2$, molar ratio of 1.5:1). To improve a film morphology, polyethylene oxide (M_v: 100 000) (2.5 mg/ml) was added to the precursor solutions. Here, the solution concentration was 0.15 M. The precursor solution was stirred overnight at 70 °C. The energy level of $CsPbX_3$ was evaluated using an ultraviolet photoemission spectroscopy (excited by He I light source, EA-125, Scienta Omicron) and atmospheric ultraviolet photoelectron spectroscopy (AC-3, Riken Keiki). The standard PL spectrum was obtained using a fluorescence spectrophotometer (Hitachi F-4500). The time-resolved photoluminescence spectra were measured using the third harmonic of a pulsed Nd:YAG laser (355 nm, 10 Hz, 0.03 mJ/cm^2) and a spectrometer (Newport MS257) equipped with a fast-gated intensified CCD camera (Andor iStar DH720).

3. Fabrication of perovskite light emitting diodes (PeLEDs) and characterization

Fabrication and measurement methods are schematically described in Figs. S6 and S7 in the supplementary material, respectively. a-ZSO ETLs were deposited on the ITO-patterned glass substrates (Flat ITO, Geomatec), using RF magnetron sputtering, where a metal shadow mask was used to pattern the a-ZSO ETL [Fig. 5(b) and Fig. S6 in the supplementary material]. UV-ozone surface treatment (SKB401Y-01, SunEnergy) was performed for 10 min before spin-coating. The substrates were transferred to an Ar-filled glovebox (UL-1000A, UNICO), where $CsPbX_3$ thin films were spin-coated (L2001A, Ossila) at 3000 rpm for 80 s and annealed at 70 °C for 10 min. Then, the samples were transferred to the air and the common electrode area was removed using acetone with a swab, followed by 120 °C annealing for 3 min. 40-nm thick a-NPD (Sigma-Aldrich), 5-nm thick MoO_x (Kojundo Chemical Lab.), and 100-nm thick Ag (Nilaco) were thermally evaporated using a metal shadow mask. The deposition rate of each material was adjusted by measuring their thickness using XRR (SmartLab, Rigaku). The fabricated PeLEDs were transferred to the Ar-filled glovebox. As shown in Fig. S7 in the supplementary material, EL intensity was determined using a luminance colorimeter (BM-7A, Topcon Corp., calibration date: November 8, 2018) without the unit conversion (the unit of BM-7A measurement is candela per meter square). The luminance–current density–voltage (L–J–V) measurement was automated by the program Labview with Keithley 2635B and BM-7A. To estimate the accurate current density (mA/cm^2), the emission area was precisely determined using a microscope. Power efficiency (lm/W) and external quantum efficiency (EQE) were calculated from the experimentally obtained luminance (cd/m^2), voltage (V), and current density (mA/cm^2), assuming a Lambertian distribution. EQE was estimated using the following equation:

$$\frac{\pi e}{Kmhc}\frac{L}{J}\left[\frac{\int F(\lambda)\,d\lambda}{\int (1/\lambda)F(\lambda)y(\lambda)d\lambda}\right].$$

K_m is the maximum luminous efficacy at 555 nm (683 lm/W). L, J, h, c, e, λ denote luminance (cd/m^2), current density (A/m^2), the plank constant, the speed of light, the electron charge and wavelength, respectively. Here, $y(\lambda)$ is the CIE photopic spectral luminous efficiency function and $F(\lambda)$ is an EL function. $F(\lambda)$ was determined from the experimentally obtained EL spectrum using multipeak fitting with Gaussian function (Fig. S8 in the supplementary material).

REFERENCES

[1]T. Jun, K. Sim, S. Iimura, M. Sasase, H. Kamioka, J. Kim, and H. Hosono, Adv. Mater. **30**, 1804547 (2018).
[2]B. O. Dabbousi, J. Rodriguez-Viejo, F. V. Mikulec, J. R. Heine, H. Mattoussi, R. Ober, K. F. Jensen, and M. G. Bawendi, J. Phys. Chem. B **101**, 9463 (1997).
[3]Q. Zhang, D. Tsang, H. Kuwabara, Y. Hatae, B. Li, T. Takahashi, S. Y. Lee, T. Yasuda, and C. Adachi, Adv. Mater. **27**, 2096 (2015).
[4]H. Kaji, H. Suzuki, T. Fukushima, K. Shizu, K. Suzuki, S. Kubo, T. Komino, H. Oiwa, F. Suzuki, A. Wakamiya, Y. Murata, and C. Adachi, Nat. Commun. **6**, 8476 (2015).
[5]C. W. Tang and S. A. VanSlyke, Appl. Phys. Lett. **51**, 913 (1987).
[6]N. Yantara, S. Bhaumik, F. Yan, D. Sabba, H. A. Dewi, N. Mathews, P. P. Boix, H. V. Demir, and S. Mhaisalkar, J. Phys. Chem. Lett. **6**, 4360 (2015).
[7]J. Song, J. Li, X. Li, L. Xu, Y. Dong, and H. Zeng, Adv. Mater. **27**, 7162 (2015).
[8]N. Wang, L. Cheng, R. Ge, S. Zhang, Y. Miao, W. Zou, C. Yi, Y. Sun, Y. Cao, R. Yang, Y. Wei, Q. Guo, Y. Ke, M. Yu, Y. Jin, Y. Liu, Q. Ding, D. Di, L. Yang, G. Xing, H. Tian, C. Jin, F. Gao, R. H. Friend, J. Wang, and W. Huang, Nat. Photonics **10**, 699 (2016).
[9]I. P. Pashuk, N. S. Pidzyrajlo, and M. G. Matsko, Sov. Phys. Solid State **23**, 1263 (1981).
[10]J. H. Cha, J. H. Han, W. Yin, C. Park, Y. Park, T. K. Ahn, J. H. Cho, and D. Y. Jung, J. Phys. Chem. Lett. **8**, 565 (2017).
[11]S. Pimputkar, J. S. Speck, S. P. DenBaars, and S. Nakamura, Nat. Photonics **3**, 180 (2009).
[12]L. Zhang, X. Yang, Q. Jiang, P. Wang, Z. Yin, X. Zhang, H. Tan, Y. M. Yang, M. Wei, B. R. Sutherland, E. H. Sargent, and J. B. You, Nat. Commun. **8**, 15640 (2017).
[13]K. Nomura, H. Ohta, A. Takagi, T. Kamiya, M. Hirano, and H. Hosono, Nature **432**, 488 (2004).
[14]J. Kim, K. Yamamoto, S. Iimura, S. Ueda, and H. Hosono, Adv. Mater. Interfaces **5**, 1801307 (2018).
[15]S. D. Stranks, G. E. Eperon, G. Grancini, C. Menelaou, M. J. P. Alcocer, T. Leijtens, L. M. Herz, A. Petrozza, and H. J. Snaith, Science **342**, 341 (2013).
[16]H. Hosono, J. Kim, Y. Toda, T. Kamiya, and S. Watanabe, Proc. Natl. Acad. Sci. **114**, 233 (2017).
[17]C. Wu, Y. Zou, T. Wu, M. Ban, V. Pecunia, Y. Han, Q. Liu, T. Song, S. Duhm, and B. Sun, Adv. Funct. Mater. **27**, 1700338 (2017).
[18]Z. Wang, Z. Luo, C. Zhao, Q. Guo, Y. Wang, F. Wang, X. Bian, A. Alsaedi, T. Hayat, and Z. Tan, J. Phys. Chem. C **121**, 28132 (2017).
[19]Y. Ling, Y. Tian, X. Wang, J. C. Wang, J. M. Knox, F. Perez-Orive, Y. Du, K. Hanson, B. Ma, and H. Gao, Adv. Mater. **28**, 8983 (2016).
[20]H. Cho, J. S. Kim, C. Wolf, Y. H. Kim, H. J. Yun, S. H. Jeong, A. Sadhanala, V. Venugopalan, J. W. Choi, C. L. Lee, R. H. Friend, and T. W. Lee, ACS Nano **12**, 2883 (2018).
[21]H. K. Seo, H. Kim, J. Lee, M. H. Park, S. H. Jeong, Y. H. Kim, S. J. Kwon, T. H. Han, S. Yoo, and T. W. Lee, Adv. Mater. **29**, 1605587 (2017).
[22]H. Cho, S. H. Jeong, M. H. Park, Y. H. Kim, C. Wolf, C. L. Lee, J. H. Heo, A. Sadhanala, N. Myoung, S. Yoo, S. H. Im, R. H. Friend, and T. W. Lee, Science **350**, 1222 (2015).
[23]Z. Wang, F. Wang, W. Sun, R. Ni, S. Hu, J. Liu, B. Zhang, A. Alsaed, T. Hayat, and Z. Tan, Adv. Funct. Mater. **28**, 1804187 (2018).
[24]T. Chiba, K. Hoshi, Y. J. Pu, Y. Takeda, Y. Hayashi, S. Ohisa, S. Kawata, and J. Kido, ACS Appl. Mater. Interfaces **9**, 18054 (2017).
[25]Z. Shi, Y. Li, S. Li, X. Li, D. Wu, T. Xu, Y. Tian, Y. Chen, Y. Zhang, B. Zhang, C. Shan, and G. Du, Adv. Funct. Mater. **28**, 1707031 (2018).
[26]K. Lin, J. Xing, L. N. Quan, F. P. G. de Arquer, X. Gong, J. Lu, L. Xie, W. Zhao, D. Zhang, C. Yan, W. Li, X. Liu, Y. Lu, J. Kirman, E. H. Sargent, Q. Xiong, and Z. Wei, Nature **562**, 245 (2018).
[27]B. Li, Y. Zhang, L. Zhang, and L. Yin, Adv. Mater. **29**, 1701221 (2017).
[28]Z. K. Tan, R. S. Moghaddam, M. L. Lai, P. Docampo, R. Higler, F. Deschler, M. Price, A. Sadhanala, L. M. Pazos, D. Credgington, F. Hanusch, T. Bein, H. J. Snaith, and R. H. Friend, Nat. Nanotechnol. **9**, 687 (2014).
[29]B. Jeong, H. Han, Y. J. Choi, S. H. Cho, E. H. Kim, S. W. Lee, J. S. Kim, C. Park, D. Kim, and C. Park, Adv. Funct. Mater. **28**, 1706401 (2018).
[30]N. K. Kumawat, A. Dey, K. L. Narasimhan, and D. Kabra, ACS Photonics **2**, 349 (2015).
[31]Y. Tian, C. Zhou, M. Worku, X. Wang, Y. Ling, H. Gao, Y. Zhou, Y. Miao, J. Guan, and B. Ma, Adv. Mater. **30**, 1707093 (2018).
[32]B. Han, B. Cai, Q. Shan, J. Song, J. Li, F. Zhang, J. Chen, T. Fang, Q. Ji, X. Xu, and H. Zeng, Adv. Funct. Mater. **28**, 1804285 (2018).
[33]Z. He, Y. Liu, Z. Yang, J. Li, J. Cui, D. Chen, Z. Fang, H. He, Z. Ye, H. Zhu, N. Wang, J. Wang, and Y. Jin, ACS Photonics **6**, 587 (2019).
[34]M. Lu, X. Zhang, Y. Zhang, J. Guo, X. Shen, W. W. Yu, and A. L. Rogach, Adv. Mater. **30**, 1804691 (2018).
[35]J. Pan, Y. Shang, J. Yin, M. D. Bastiani, W. Peng, I. Dursun, L. Sinatra, A. M. El-Zohry, M. N. Hedhili, A. H. Emwas, O. F. Mohammed, Z. Ning, and O. M. Bakr, J. Am. Chem. Soc. **140**, 562 (2018).
[36]T. Chiba, Y. Hayashi, H. Ebe, K. Hoshi, J. Sato, S. Sato, Y. J. Pu, S. Ohisa, and J. Kido, Nat. Photonics **12**, 681 (2018).
[37]X. Zhang, C. Sun, Y. Zhang, H. Wu, C. Ji, Y. Chuai, P. Wang, S. Wen, C. Zhang, and W. W. Yu, J. Phys. Chem. Lett. **7**, 4602 (2016).
[38]G. Li, F. W. R. Rivarola, N. J. L. K. Davis, S. Bai, T. C. Jellicoe, F. de la Peña, S. Hou, C. Ducati, F. Gao, R. H. Friend, N. C. Greenham, and Z. K. Tan, Adv. Mater. **28**, 3528 (2016).
[39]D. N. Congreve, M. C. Weidman, M. Seitz, W. Paritmongkol, N. S. Dahod, and W. A. Tisdale, ACS Photonics **4**, 476 (2017).
[40]Z. Chen, C. Zhang, X. F. Jiang, M. Liu, R. Xia, T. Shi, D. Chen, Q. Xue, Y. J. Zhao, S. Su, H. L. Yip, and Y. Cao, Adv. Mater. **29**, 1603157 (2017).
[41]S. Kumar, J. Jagielski, S. Yakunin, P. Rice, Y. C. Chiu, M. Wang, G. Nedelcu, Y. Kim, S. Lin, E. J. G. Santos, M. V. Kovalenko, and C. J. Shih, ACS Nano **10**, 9720 (2016).
[42]M. K. Gangishetty, S. Hou, Q. Quan, and D. N. Congreve, Adv. Mater. **30**, 1706226 (2018).